MIMO Radar With Array Manifold Extenders

HE REN
ATHANASSIOS MANIKAS, Senior Member, IEEE
Imperial College London, London, U.K.

This article is concerned with the problem of multitarget parameter estimation in arrayed multiple-input multiple-output (MIMO) radar. In particular, the radar operates in the presence of moving targets, where the parameters of interests to be estimated for each target are the relative delay, Doppler frequency, direction-of-arrival (DOA) and complex path coefficients (or target's radar cross section). Using the novel concept of "array manifold extender," the dimensionality of the observation space increases from N to $N\mathcal{N}_{\text{ext}}$, making the radar more powerful than conventional MIMO radar systems by handling more complex targets and estimating their parameters with increased accuracy. Two "manifold extenders" are proposed in this article in conjunction with a novel spatiotemporal subspace-type framework for estimating the target parameters. The performance of proposed framework is examined using computer simulation studies.

Manuscript received March 6, 2018; revised October 3, 2018, April 8, 2019, and August 5, 2019; released for publication August 13, 2019. Date of publication December 9, 2019; date of current version June 9, 2020.

DOI. No. 10.1109/TAES.2019.2940307

Refereeing of this contribution was handled by B. Lao.

Authors' address: H. Ren and A. Manikas are with the Department of Electrical and Electronic Engineering, Imperial College London SW7 2AZ, London, U.K. E-mail: (renhe2046@gmail.com; a.manikas@imperial.ac.uk). *(Corresponding author: A. Manikas.)*

NOTATION

a, A	Scalar.
$\underline{a}$, $\underline{A}$	Column Vector.
$\mathbb{A}$	Matrix.
$\underline{0}_N$	$N \times 1$ vector of zeros.
$\underline{1}_N$	$N \times 1$ vector of ones.
$\mathbb{I}_N$	Identity matrix of size $N \times N$.
$\mathbb{O}_{M\times N}$	Matrix of zeros of size $M \times N$.
$(\cdot)^*$	Complex conjugate.
$(\cdot)^\#$	Pseudoinverse.
$(\cdot)^T$, $(\cdot)^H$	Transpose, Hermitian transpose.
$\|\cdot\|$	Euclidean norm.
$\lceil a \rceil$	Integer ceiling of scalar a.
$\odot$	Hadamard product.
$\otimes$	Kronecker product.
$\boxtimes$	Khatri–Rao product.
$\mathcal{E}\{\cdot\}$	Expectation operator.
$\underline{A}^b$	Element by element power of $\underline{A}$.
$\text{Tr}\{\mathbb{A}\}$	Trace of $\mathbb{A}$.
$\exp(\underline{A})$	Element-wise exponential of vector $\underline{A}$.
$\text{vec}\{\mathbb{A}\}$	Column-wise vectorization of $\mathbb{A}$.
$\text{diag}\{\underline{A}\}$	The diagonal matrix whose diagonal elements are the elements of $\underline{A}$.
$\underline{\text{diag}}\{\mathbb{A}\}$	The column vector with elements the diagonal elements of $\mathbb{A}$.
$\text{rank}\{\mathbb{A}\}$	Rank of matrix $\mathbb{A}$.
$\mathcal{C}$	Field of complex numbers.
$\mathcal{R}$	Set of real numbers.

I. INTRODUCTION

Many direction-of-arrival (DOA) and path gain estimation algorithms for conventional array system can be applied in the arrayed multiple-input multiple-output (MIMO) radar. Least squares (LS) [1], Capon [2], [3], and amplitude and phase estimation (APES) [4], [5] are joint approaches for DOAs and complex path coefficients. The comparison in [6] shows that the Capon provides accurate DOA estimation while APES outperforms the other methods for accurate complex path estimation. To obtain the joint benefits of both, in [7], [8], the Capon-and-APES (CAPES) method is proposed, where the DOAs of targets is estimated by Capon's method and estimates of the path gains are provided via the APES method. Furthermore, a generalized likelihood ratio test is proposed in [9] for the DOA estimation of multiple targets, particularly in hostile environments and it is well known for its good antijamming capabilities. In [10], the Capon-and-AML (CAML) algorithm is presented, which utilizes Capon for the DOA estimation and an approximate maximum likelihood (AML) method for the path gain estimation. However, the above methods are not capable of handling moving targets and the number of Degree-of-Freedom (DoF) of these methods are limited by the number of receiver's array elements.

Note that, in the modern multiantenna wireless systems, the explosive demand for operating in more dense targets/signal environments with higher resolution and greater estimation accuracy requires more DoF. The DoF is defined

as the maximum number of signals that can be observed in the systems observation space, where its dimensionality is restricted by the number of radar's antenna array elements, which consequently restricts the DoF. Furthermore, the "array manifold," which is one of the most important concepts in array signal processing is embedded in the observation space. The "array manifold" is a function of the array geometry and is a mathematical object (curve, surface, etc.) which is the locus of all array response vectors [11]–[13].

One way to achieve more DoF is to increase the number of the receiver's array elements, which in practice requires relatively high cost as it needs to install more hardware. Alternatively, this can be done using the concept of the "extended manifolds" by including in the manifold's description additional system and channel parameters, such as Doppler frequency, polarisation, number of carriers etc. [13]. The spatiotemporal array (STAR) manifold and its alternative forms, such as Doppler STAR, are the most common types of manifold extenders, which integrate both "space" and "time" in a single manifold vector. Other approaches are the space-time adaptive processing (STAP) techniques which use the space-time steering vector in the space-time look-direction [14], [15]. Furthermore, having more DoF implies that the radar system is able to handle more targets and clutter effect with greater detection and resolution capabilities and with increased target-parameter estimation accuracy [3].

Meanwhile for a MIMO radar, the available DoF at transmitter array can be increased up to $\bar{N}$ due to the orthogonality between the transmitted array signals [16], [17]. These extra DoF are not easy to be directly utilized by the receiver of the MIMO radar, and the *virtual spatiotemporal array* concept is also considered in this article, where the transmitter's DoF is incorporated into the extended manifold vectors (on top of the spatiotemporal manifold vector) to increase even further the observation space and consequently the DoFs.

The rest of the article is organized as follows: In Sections II, the parametric modeling for MIMO radar is presented, with the radar operating in the presence of multiple moving targets and ground clutter. Section III focuses on the concept of the extended manifold vector, where two forms of array manifold extenders are presented. By employing these two extenders in conjunction with the proposed spatiotemporal modeling, a novel subspace-based estimation approach is proposed in Section IV, for estimating the target parameters including DOAs, delays, velocities and complex path coefficients(i.e. target's radar cross section). A number of computer simulation studies are presented in Section V to evaluate the performance of the proposed approach. This article is finally concluded in Section VI.

II. GENERAL ARRAYED MIMO RADAR SYSTEM MODEL

Consider a MIMO radar system having antenna arrays at both its transmitter (Tx) and receiver (Rx) with $\bar{N}$ and N elements respectively. The Tx and Rx arrays are located close to each other having a common Cartesian coordinate

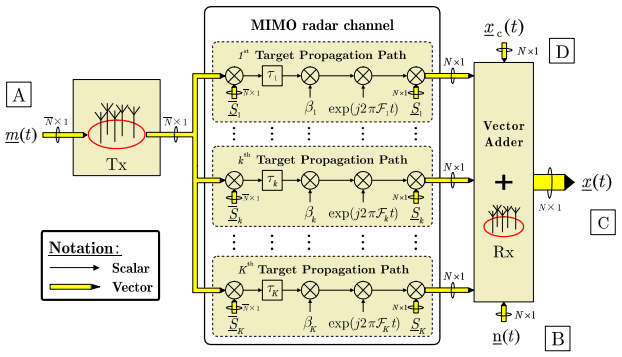

Fig. 1. Baseband propagation model of the MIMO radar system in the presence of K point targets implemented with M patches of clutter reflections.

system (colocated MIMO Radar). This configuration, based on antenna arrays, is known as an arrayed MIMO radar system. Without loss of generality, both Tx and Rx arrays are assumed to be fully calibrated. The radar is assumed to operate in the presence of K moving targets and ground clutters in the far field of the radar platform (aperture), which implies plane wave propagation.

A. Transmitted Signal Modeling

Fig. 1 illustrates the basic structure of the MIMO radar system where a baseband vector signal $\underline{m}(t)$ (see point A)

$$\underline{m}(t) = \left[m_1(t), m_2(t), \ldots, m_{\bar{N}}(t)\right]^T \in \mathcal{C}^{\bar{N}\times 1} \tag{1}$$

is transmitted with a carrier frequency F_c using a Tx antenna array of $\bar{N}$ elements. This transmitted signal is based on a sequence of orthogonal vector[1] symbols $\{\underline{a}[n] \in \mathcal{C}^{\bar{N}\times 1}, \forall n\}$, where the duration of each symbol $\underline{a}[n]$ is equal to T_{symb}. Assuming that $\mathcal{N}_{\text{symb}}$ symbols are transmitted, these can be represented by the matrix $\mathbb{M}$ defined as follows:

$$\mathbb{M} \triangleq \left[\underline{a}\,[1]\,, \underline{a}\,[2]\,, \ldots, \underline{a}\,[n]\,, \ldots, \underline{a}\left[\mathcal{N}_{\text{symb}}\right]\right] \in \mathcal{C}^{\bar{N}\times\mathcal{N}_{\text{symb}}} \tag{2}$$

where

$$\mathbb{M}\mathbb{M}^H = \mathbb{I}_{\bar{N}}. \tag{3}$$

Each column of the matrix $\mathbb{M}$ is processed by a sequence[2] of $2\mathcal{N}_c$ chips with the chip duration T_c defined by the vector $\underline{c} \in \mathcal{R}^{2\mathcal{N}_c\times 1}$ as follows: [3]

$$\underline{c} \triangleq \Big[\alpha\,[1]\,, \alpha\,[2]\,, \ldots, \alpha\,[\mathcal{N}_c]\,, \underbrace{\alpha\,[\mathcal{N}_c+1]\,, \ldots, \alpha\,[2\mathcal{N}_c]}_{=\underline{0}^T_{\mathcal{N}_c}}\Big]^T \tag{4}$$

and thus a new transmitted sequence represented by the columns of the following matrix can be formed:

$$\mathbb{M}\otimes\underline{c}^T = \left[\underline{a}\,[1]\,\underline{c}^T, \underline{a}\,[2]\,\underline{c}^T, \ldots, \underline{a}\left[\mathcal{N}_{\text{symb}}\right]\underline{c}^T\right] \in \mathcal{C}^{\bar{N}\times 2\mathcal{N}_c\mathcal{N}_{\text{symb}}}$$

[1] the elements of the vector $\underline{a}[n]$ are transmitted in parallel.

[2] e.g. an m-sequence of period $\mathcal{N}_c$ padded with $\mathcal{N}_c$ zeros. Note that m-sequences have excellent autocorrelation properties

[3] Without loss of generality, the delay spread of the targets is assumed to be not greater than $\mathcal{N}_c T_c$.

where the transmitted sequence associated with the n^{th} symbol is of duration $T_{\text{symb}} = 2\mathcal{N}_c T_c$.

By using a pulse-shaping filter $p(t)$ of duration T_c, the transmitted sequence at time t can be transformed to the signal $\underline{m}(t)$ and represented as follows:

$$\underline{m}(t) = \sum_{n=1}^{\mathcal{N}_{\text{symb}}} \underline{\mathrm{a}}[n] \sum_{i=1}^{2\mathcal{N}_c} \alpha[i]\, p\left(t-(n-1)\,2\mathcal{N}_c T_c-(i-1)\,T_c\right)$$

with $n = 1, 2, \ldots, \mathcal{N}_{\text{symb}}$ representing the indices of the transmitted symbol and $i = 1, 2, \ldots, 2\mathcal{N}_c$ denoting the chips indices.

B. MIMO Radar Channel Modeling

Fig. 1 also shows that there are K targets (K target parallel propagation paths), where for the kth target, the transmitted vector signal $\underline{m}(t)$ is successively weighted by

1) the Tx manifold vector $\underline{\bar{S}}_k \triangleq \underline{\bar{S}}(\theta_k, \phi_k) \in \mathcal{C}^{\bar{N}\times 1}$, i.e.,

$$\underline{\bar{S}}_k(\theta_k, \phi_k) = \exp\left(+j\frac{2\pi F_{\text{c}}}{c}\left[\bar{\underline{r}}_x, \bar{\underline{r}}_y, \bar{\underline{r}}_z\right]\underline{u}(\theta_k, \phi_k)\right) \tag{5}$$

   where
   - the $(\bar{N}\times 3)$ matrix $[\bar{\underline{r}}_x, \bar{\underline{r}}_y, \bar{\underline{r}}_z]$ denotes the Cartesian coordinates the Tx array elements;
   - θ_k and ϕ_k denote the azimuth and elevation angles of the kth target respectively;
   - $\underline{u}(\theta_k, \phi_k)$ is a unity vector pointing towards the kth target's direction;
2) the propagation path delay τ_k with respect to the reference clock;
3) the complex gain β_k which is related to the RCS of the kth target;
4) the Doppler shift $\exp(j2\pi\mathcal{F}_k t)$ where $\mathcal{F}_k$ denotes the Doppler frequency of the kth target, which can be expressed as a function of radial velocity v_k:

$$\mathcal{F}_k \triangleq -\frac{2v_k F_{\text{c}}}{c} \tag{6}$$

   with F_{c} representing the carrier frequency and c is the speed of light;
5) the Rx manifold vector $\underline{S}_k \triangleq \underline{S}(\theta_k, \phi_k) \in \mathcal{C}^{N\times 1}$ with

$$\underline{S}_k(\theta_k, \phi_k) = \exp\left(-j\frac{2\pi F_{\text{c}}}{c}\left[\underline{r}_x, \underline{r}_y, \underline{r}_z\right]\underline{u}(\theta_k, \phi_k)\right) \tag{7}$$

   where $[\underline{r}_x, \underline{r}_y, \underline{r}_z]$ denotes the Cartesian coordinates of the Rx array elements.

Furthermore, at Point D, $\underline{x}_{\text{c}}(t)$ denotes the clutter vector signal, where typical clutter objects are buildings, trees and hills that are dispersedly distributed. The modeling for the clutter signal $\underline{x}_{\text{c}}$ is not in any specified parametric form in this article, but only its statistics will be required.

Finally, at Point C, $\underline{x}(t)$ is the received vector signal, which is addition of the returns of the targets plus clutter plus noise $\underline{\mathrm{n}}(t)$. As a result, the overall received signal vector $\underline{x}(t)$ at receiver can be written as

$$\begin{aligned}\underline{x}(t) &= [x_1(t), x_2(t), \ldots, x_N(t)]^T \in \mathcal{C}^{N\times 1}\\ &= \sum_{k=1}^{K}\beta_k \exp(j2\pi\mathcal{F}_k t)\,\underline{S}(\theta_k, \phi_k)\,\underline{\bar{S}}^H(\theta_k, \phi_k)\\ &\quad\times \underline{m}(t-\tau_k) + \underline{x}_{\text{c}}(t) + \underline{\mathrm{n}}(t)\end{aligned} \tag{8}$$

where the noise vector $\underline{\mathrm{n}}(t) \in \mathcal{C}^{N\times 1}$ (see point B in Fig. 1) is assumed to be complex isotropic Gaussian noise of zero mean and covariance matrix $\mathbb{R}_{\text{nn}} = \sigma_{\text{n}}\mathbb{I}_N$, that is

$$\mathbb{R}_{\text{nn}} \triangleq \mathcal{E}\left\{\underline{\mathrm{n}}(t)\underline{\mathrm{n}}^H(t)\right\} = \sigma_{\text{n}}^2\mathbb{I}_N. \tag{9}$$

with σ_{n}^2 denoting the unknown noise power. Without loss of generality, the independence between the clutter and noise is assumed.

C. Receiver Signal Discretization

By discretizing the received signal $\underline{x}(t)$ given by (8) and collecting data corresponding to $\mathcal{N}_{\text{symb}}$ transmitted symbols, the data matrix $\mathbb{X} \in \mathcal{C}^{N\times 2\mathcal{N}_c\mathcal{N}_{\text{symb}}}$ is formed as follows:

$$\mathbb{X} \triangleq \left[\mathbb{X}[1], \mathbb{X}[2], \ldots, \mathbb{X}[n], \ldots, \mathbb{X}\left[\mathcal{N}_{\text{symb}}\right]\right] \tag{10}$$

where the data submatrix $\mathbb{X}[n] \in \mathcal{C}^{N\times 2\mathcal{N}_c}$ can be expressed as a function of the nth transmitted symbol $\underline{\mathrm{a}}[n]$, the static clutter matrix $\mathbb{X}_{\text{c}}[n]$ and noise matrix $\mathbb{N}[n]$ as follows:

$$\begin{aligned}\mathbb{X}[n] &\triangleq \mathbb{X}_{\text{t}}[n] + \mathbb{X}_{\text{c}}[n] + \mathbb{N}[n]\\ &= \sum_{k=1}^{K}\beta_k \exp\left(j2\pi n\mathcal{F}_k T_{\text{symb}}\right)\underline{S}_k\underline{\bar{S}}_k^H\,\underline{\mathrm{a}}[n]\\ &\quad\times\left(\mathbb{J}^{l_k}\underline{\mathfrak{c}}\odot\underline{\mathcal{F}}_{\text{chips},k}\right)^T + \mathbb{X}_{\text{c}}[n] + \mathbb{N}[n].\end{aligned} \tag{11}$$

D. Clutter Preprocessing

The disturbance such as ground clutter is not white Gaussian but its probability density function may follow different distributions, such as *Weibull, Log-Weibull, and K-distribution*. This will reduce the superresolution capabilities and accuracy of subspace-type parameters estimation methods, mainly because the clutter-plus-noise is not going to be white (isotropic) anymore. Consequently, it is intuitive to mitigate the ground clutter in a similar way as the color-noise whitening process in signal processing [18]–[20].

In this context, the second-order statistics of $\underline{x}(t)$ can be expressed as:

$$\begin{aligned}\mathbb{R}_{xx} &= \mathcal{E}\left\{\underline{x}(t)\underline{x}^H(t)\right\}\\ &= \mathcal{E}\left\{\underline{x}_{\text{t}}(t)\underline{x}_{\text{t}}^H(t)\right\} + 2\text{Re}\mathcal{E}\left(\underline{x}_{\text{t}}(t)\underline{x}_{\text{c}}^H(t)\right)\\ &\quad+\underbrace{\mathcal{E}\left\{\underline{x}_{\text{c}}(t)\underline{x}_{\text{c}}^H(t)\right\} + \mathcal{E}\left\{\underline{\mathrm{n}}(t)\underline{\mathrm{n}}^H(t)\right\}}_{\triangleq\mathbb{R}_{\text{c,n}}}.\end{aligned} \tag{12}$$

In (12), due to the good correlation properties of transmit signals, it is assumed that the clutter and the targets are located in different range bins. This implies that $\mathcal{E}(\underline{x}_{\text{t}}(t)\underline{x}_{\text{c}}^H(t)) \approx \mathbb{O}_N$, i.e., the covariance matrix between

TABLE I
Redefining Parameters After Clutter-Plus-Noise Whitening

Original Notations	Redefined Parameters (Clutter)
$\underline{x}(t), \underline{x}[n]$	$\underline{x}(t) \triangleq \mathbb{T}\underline{x}(t),\ \underline{x}[n] \triangleq \mathbb{T}\underline{x}[n]$
$\mathbb{X}$	$\mathbb{X} \triangleq \mathbb{T}\mathbb{X}$
$\mathbb{R}_{xx}$	$\mathbb{R}_{xx} \triangleq \mathbb{T}\mathbb{R}_{xx}\mathbb{T}$
$\underline{S}$	$\underline{S} \triangleq \mathbb{T}\underline{S}$
$\mathbb{N}$	$\mathbb{N} \triangleq \mathbb{T}\mathbb{N}$

the echo from target and clutter can be ignored. Furthermore, the matrix $\mathbb{R}_{\mathrm{c,n}}$ in (12) denotes the covariance matrix of the clutter plus noise and can be decomposed by eigendecomposition

$$\mathbb{R}_{\mathrm{c,n}} = \mathbb{E}\mathbb{D}^{\frac{1}{2}}\mathbb{D}^{\frac{1}{2}}\mathbb{E}^H \tag{13}$$

where $\mathbb{E} \in \mathcal{C}^{N\times N}$ is a unitary matrix composed of the N eigenvectors and

$$\mathbb{D} \triangleq \mathrm{diag}\left\{[\lambda_1, \lambda_2, \ldots, \lambda_n, \ldots, \lambda_N]^T\right\} \tag{14}$$

is a diagonal matrix of the eigenvalues where λ_n corresponding to nth eigenvector at the corresponding column of $\mathbb{E}$.

With reference to (13) let us define a transformation matrix $\mathbb{T}$

$$\mathbb{T} \triangleq \mathbb{D}^{-\frac{1}{2}}\mathbb{E}^H \in \mathcal{C}^{N\times N}. \tag{15}$$

Then, by applying $\mathbb{T}$ to the received signal, the clutter term can be "isotropically whiten," which implies the covariance matrix of clutter-plus-noise $\mathbb{R}_{\mathrm{c,n}}$ is effectively transformed into an identity matrix. Indeed,

$$\begin{aligned}\mathbb{T}\mathbb{R}_{xx}\mathbb{T}^H &= \mathbb{D}^{-\frac{1}{2}}\mathbb{E}^H \underbrace{\mathcal{E}\left\{\underline{x}_{\mathrm{t}}(t)\underline{x}_{\mathrm{t}}^H(t)\right\}}_{\triangleq\mathbb{R}_{\mathrm{tt}}} \mathbb{E}\mathbb{D}^{-\frac{1}{2}} \\ &\quad + 2\mathbb{D}^{-\frac{1}{2}}\mathbb{E}^H \mathrm{Re}\underbrace{\left(\mathcal{E}\left\{\underline{x}_{\mathrm{t}}(t)\underline{x}_{\mathrm{c}}^H(t)\right\}\right)}_{\triangleq\mathbb{R}_{\mathrm{t,c}}} \mathbb{E}\mathbb{D}^{-\frac{1}{2}} \\ &\quad + \underbrace{\mathbb{D}^{-\frac{1}{2}}\mathbb{E}^H\mathbb{E}\mathbb{D}^{\frac{1}{2}}\mathbb{D}^{\frac{1}{2}}\mathbb{E}^H\mathbb{E}\mathbb{D}^{-\frac{1}{2}}}_{\triangleq\mathbb{T}(\mathbb{R}_{\mathrm{cc}}+\mathbb{R}_{\mathrm{nn}})\mathbb{T}^H=\mathbb{I}_N}. \end{aligned} \tag{16}$$

Using the data covariance matrix corresponding to $L = 2\mathcal{N}_c\mathcal{N}_{\mathrm{symb}}$ snapshots, (16) can be rewritten as

$$\begin{aligned}\mathbb{T}\mathbb{R}_{xx}\mathbb{T}^H &= \frac{1}{L}\mathbb{T}\mathbb{X}\mathbb{X}^H\mathbb{T}^H \\ &= \frac{1}{L}\mathbb{T}\mathbb{X}_{\mathrm{t}}\mathbb{X}_{\mathrm{t}}^H\mathbb{T}^H + \frac{2}{L}\mathbb{T}\mathrm{Re}\underbrace{\left(\mathbb{X}_{\mathrm{t}}\mathbb{X}_{\mathrm{c}}^H\right)}_{\simeq\mathbb{O}_N}\mathbb{T}^H \\ &\quad + \underbrace{\frac{1}{L}\mathbb{T}\left(\mathbb{X}_{\mathrm{c}}\mathbb{X}_{\mathrm{c}}^H + \mathbb{N}\mathbb{N}^H\right)\mathbb{T}^H}_{\simeq\mathbb{I}_N} \end{aligned} \tag{17}$$

where $\mathbb{T}$ can be estimated using the data collected in the absence of the targets.

In the rest of the article, for notational convenience, some parameters are redefined as shown in Table I. Note that in the absence of clutter, the transformation matrix $\mathbb{T}$ is simplified to an identity matrix.

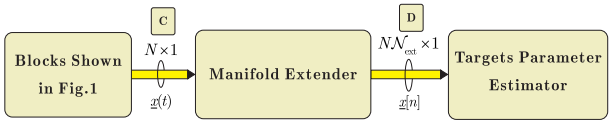

Fig. 2. System with manifold extender.

III. EXTENDED ARRAY MANIFOLDS

After clutter preprocessing, the $(N \times 1)$ signal $\underline{x}(t)$ is fed to a "manifold extender," which includes a discretizer. With reference to Fig. 2, note that the signal $\underline{x}(t)$ at the input of the "manifold extender" is a function of the conventional manifold vectors $\underline{S}_k$, $\forall k$(that is for all the targets). However the signal $\underline{x}[n]$ at the output of the "manifold extender" is a function [21] of the "extended manifolds", $\underline{h}_k \in \mathcal{C}^{N\mathcal{N}_{\mathrm{ext}}\times 1}$, $\forall k$, where $\mathcal{N}_{\mathrm{ext}}$ is different for different types of manifold extenders.

In this article, two manifold extenders are presented. The first will extend the observation space from N to $2N\mathcal{N}_c$. In this case, the extended manifold is known as "Doppler-STAR manifold," where STAR-manifold stands for SpatioTemporal-ARray manifold. The second extender extends the observation space even further by transferring the Tx-array to the receiver, creating a new observation space of $2N\bar{N}\mathcal{N}_c$ dimensions. In this case, the extended manifold is known as the virtual-SIMO STAR manifold vector.

A. Doppler-STAR Manifold Extender

With reference to Appendix-A, the discretized signal at the output of the first manifold extender can be expressed as follows:

$$\underline{x}\,[n] = \sum_{k=1}^{K}\beta_k\,\mathcal{F}_{\mathrm{symb},k}\,[n]\;\underline{h}_k\,\bar{\underline{S}}_k^H\,\underline{\mathrm{a}}\,[n] + \underline{\mathrm{n}}\,[n] \tag{18}$$

where, for the kth target

$$\mathcal{F}_{\mathrm{symb},k}\,[n] = \exp\left(j2\pi n T_c\mathcal{F}_k T_{\mathrm{symb}}\right) \tag{19}$$

is the Doppler effects over the nth symbol and $\underline{h}_k \in \mathcal{C}^{2\mathcal{N}_c N\times 1}$ is the "Doppler Spatiotemporal Array" manifold defined as follows:

$$\begin{aligned}\underline{h}_k &\triangleq \underline{h}\,(\theta_k, \phi_k, l_k, \mathcal{F}_k) \\ &\triangleq \underline{S}_k\,(\theta_k, \phi_k) \otimes \left(\mathbb{J}^{l_k}\underline{\mathfrak{c}} \odot \underline{\mathcal{F}}_{\mathrm{chip},k}\right) \end{aligned} \tag{20}$$

with

1) l_k denoting the quantized delay associated with kth target

$$l_k \triangleq \left\lceil \frac{\tau_k}{T_c} \right\rceil \bmod \mathcal{N}_c. \tag{21}$$

2) $\underline{\mathcal{F}}_{\text{chip},k} \in \mathcal{C}^{2\mathcal{N}_c \times 1}$ represents the Doppler effects vector over the $2\mathcal{N}_c$ chips, given as follows:

$$\underline{\mathcal{F}}_{\text{chip},k} = \exp\left(j2\pi \mathcal{F}_k \begin{bmatrix} 0 \\ 1 \\ \vdots \\ 2\mathcal{N}_c - 1 \end{bmatrix} T_c \right). \tag{22}$$

3) $\mathbb{J}$ is a shifting matrix [22] defined as follows:

$$\mathbb{J} \triangleq \begin{bmatrix} \underline{0}^T_{2\mathcal{N}_c-1} & 0 \\ \mathbb{I}_{2\mathcal{N}_c-1} & \underline{0}_{2\mathcal{N}_c-1} \end{bmatrix} \in \mathcal{R}^{2\mathcal{N}_c \times 2\mathcal{N}_c}, \tag{23}$$

which has the property that every time the matrix $\mathbb{J}$ (or $\mathbb{J}^T$) operates on a column vector, it downshifts (or upshifts) the elements of the vector by one. For example, for the target with delay l, by operating the $\mathbb{J}^l$ on its message vector will downshift the vector-elements by l units.

Further, (18) can be rewritten in a more compact form as follows:

$$\underline{x}[n] = \mathbb{H}\text{diag}\left(\underline{\beta}\right)\left[\underline{\mathcal{F}}_{\text{symb}}[n] \odot \left(\bar{\mathbb{S}}^H \underline{\text{a}}[n]\right)\right] + \underline{\text{n}}[n] \tag{24}$$

where

$$\begin{cases} \bar{\mathbb{S}} \triangleq \left[\bar{\underline{S}}_1, \bar{\underline{S}}_2, \ldots, \bar{\underline{S}}_K\right] \in \mathcal{C}^{\bar{N} \times K} \\ \underline{\beta} \triangleq [\beta_1, \beta_2, \ldots, \beta_K]^T \in \mathcal{C}^{K \times 1} \\ \underline{\mathcal{F}}_{\text{symb}}[n] \triangleq \exp\left(j2\pi \begin{bmatrix} \mathcal{F}_1 \\ \mathcal{F}_2 \\ \vdots \\ \mathcal{F}_K \end{bmatrix} n T_{\text{symb}} \right) \in \mathcal{C}^{K \times 1} \end{cases}$$

and

$$\mathbb{H} = \left[\underline{h}_1, \underline{h}_2, \ldots, \underline{h}_k, \ldots, \underline{h}_K\right] \in \mathcal{C}^{K \times 1}. \tag{25}$$

That is, the matrix $\mathbb{H}$ contains as columns the Doppler STAR manifold vectors of all the K targets.

Based on the above, the data matrix $\mathbb{X}_{\text{ST}}$ can be expressed as follows:

$$\begin{aligned} \mathbb{X}_{\text{ST}} &= \left[\underline{x}[1], \underline{x}[2], \ldots, \underline{x}[n], \ldots, \underline{x}\left[\mathcal{N}_{\text{symb}}\right]\right] \\ &= \mathbb{H}\text{diag}\left(\underline{\beta}\right)\left[\mathbb{F} \odot \left(\bar{\mathbb{S}}^H \mathbb{M}\right)\right] + \mathbb{N}_{\text{ST}} \end{aligned} \tag{26}$$

where $\mathbb{N}_{\text{ST}} = [\underline{\text{n}}[1], \underline{\text{n}}[2], \ldots, \underline{\text{n}}[n], \ldots, \underline{\text{n}}[\mathcal{N}_{\text{symb}}]]$.

As a result, the second-order statistics $\mathbb{R}_{xx,\text{ST}}$ of $\underline{x}[n]$ is given as follows:

$$\begin{aligned} \mathbb{R}_{xx,\text{ST}} &= \frac{1}{\mathcal{N}_{\text{symb}}} \mathbb{X}_{\text{ST}} \mathbb{X}^H_{\text{ST}} \\ &= \frac{1}{\mathcal{N}_{\text{symb}}} \mathbb{H}\left[\left(\mathbb{F}\mathbb{F}^H\right) \odot \left(\bar{\mathbb{S}}\bar{\mathbb{S}}^H\right) \odot \left(\underline{\beta}\underline{\beta}^H\right)\right] \mathbb{H}^H \\ &\quad + \underbrace{\frac{1}{\mathcal{N}_{\text{symb}}} \mathbb{N}_{\text{ST}} \mathbb{N}^H_{\text{ST}}}_{\triangleq \mathbb{R}_{\text{nn,ST}}} \end{aligned} \tag{27}$$

where (3) has been used and the matrix $\mathbb{F}$ is defined as

$$\mathbb{F} \triangleq \left[\underline{\mathcal{F}}_{\text{symb}}[1], \underline{\mathcal{F}}_{\text{symb}}[2], \ldots, \underline{\mathcal{F}}_{\text{symb}}[n], \ldots, \underline{\mathcal{F}}_{\text{symb}}\left[\mathcal{N}_{\text{symb}}\right]\right]. \tag{28}$$

Note that, theoretically, the noise covariance matrix is

$$\begin{aligned} \mathbb{R}_{\text{nn,ST}} &= \mathcal{E}\left\{\underline{\text{n}}[n]\underline{\text{n}}^H[n]\right\} \\ &= \sigma^2_{\text{n}} \mathbb{I}_{2N\mathcal{N}c}. \end{aligned}$$

It is clear by just observing the dimensions of the covariance matrix $\mathbb{R}_{xx}$ given by (27), the dimensionality of the observation space is $2\mathcal{N}_c N$ and this implies that the radar can operate in a more dense target environment that a conventional MIMO radar where the observation space has dimensionality equal to N (number of Rx antennas).

B. Virtual Spatiotemporal Manifold Extender

With reference to (18) in the previous section, the transmitter's manifold vector associated with the kth target, $\bar{\underline{S}}_k$, is linearly combined by the transmitted symbols $\underline{\text{a}}[n]$ to form a directional scalar term and this prohibits the Tx geometry to be exploited at the radar's receiver. In this section, the transmitted sequence $\mathbb{M}$, which is perfectly known to the radar's receiver, is utilized here to exploit the Tx array geometry to increase even further the dimensionality of the observation space and consequently the DoF.

Indeed, the new data vector $\underline{x}_{\text{v}}[n]$, defined as virtual-spatiotemporal data vector, can be formed as follows (see Appendix B):

$$\begin{aligned} \underline{x}_{\text{v}}[n] &\triangleq \text{vec}\left\{\underline{x}[n]\underline{\text{a}}^H[n]\right\} \in \mathcal{C}^{2\mathcal{N}_c N \bar{N} \times 1} \\ &= \sum_{k=1}^{K} \beta_k \text{vec}\left\{\mathcal{F}_{\text{symb},k}[n]\left(\underline{S}_k \otimes \left(\mathbb{J}^{l_k}\underline{\text{c}} \odot \underline{\mathcal{F}}_{\text{chip},k}\right)\right)\right. \\ &\quad \left. \times\ \bar{\underline{S}}^H_k\, \underline{\text{a}}[n]\underline{\text{a}}^H[n]\right\} \\ &= \sum_{k=1}^{K} \beta_k \mathcal{F}_{\text{symb},k}[n]\, \mathbb{A}[n]\, \underline{h}_{\text{v},k} + \underline{\text{n}}_{\text{v}}[n] \end{aligned} \tag{29}$$

where

$$\mathbb{A}[n] = \left(\underline{\text{a}}[n]\underline{\text{a}}^H[n]\right)^T \otimes \mathbb{I}_{2\mathcal{N}_c N} \in \mathcal{C}^{2\mathcal{N}_c N \bar{N} \times 2\mathcal{N}_c N \bar{N}}. \tag{30}$$

In (29), the Tx array geometry is exploited at the receiver by the extended manifold vector $\underline{h}_{\text{v},k}$,

$$\underline{h}_{\text{v},k} \triangleq \bar{\underline{S}}^*_k \otimes \underbrace{\underline{S}_k \otimes \left(\mathbb{J}^{l_k}\underline{\text{c}} \odot \underline{\mathcal{F}}_{\text{chip},k}\right)}_{\underline{h}_k} \in \mathcal{C}^{2\mathcal{N}_c N \bar{N} \times 1}, \tag{31}$$

which is known as the virtual spatiotemporal manifold vector of the kth target. From (31) it is clear that $\underline{h}_{\text{v},k}$ is a function of both the Tx and Rx array geometries, DOA/DOD, delay, and Doppler frequency of the kth target. In fact, the extra term of the transmitter array manifold has been integrated with the 1st manifold extender and provides $\bar{N}$ additional entries, which increases the receiver's observation space by $\bar{N}$ additional dimensions. Consequently this

may be used to provide a significant improvement regarding the system capabilities (see [13]).

It is important to point out that in (29), $\underline{\mathrm{n}}_{\mathrm{v}}[n]$ is the virtual noise, i.e.

$$\underline{\mathrm{n}}_{\mathrm{v}}[n] \triangleq \underline{\mathrm{a}}^{*}[n] \otimes \underline{\mathrm{n}}[n]$$

and its theoretical covariance matrix is given as follows:

$$\begin{aligned}\mathbb{R}_{\mathrm{n_v n_v}} &\triangleq \mathcal{E}\left\{\underline{\mathrm{n}}_{\mathrm{v}}[n]\,\underline{\mathrm{n}}_{\mathrm{v}}^{H}[n]\right\} \\ &= \sigma_{\mathrm{n}}^{2}\mathbb{I}_{2\mathcal{N}_c N\bar{N}}.\end{aligned}$$

Note that (29) can be rewritten in a more compact form as

$$\underline{x}_{\mathrm{v}}[n] = \mathbb{A}[n]\,\mathbb{H}_{\mathrm{v}}\mathrm{diag}\left\{\underline{\mathcal{F}}_{\mathrm{symb}}[n]\right\}\underline{\beta} + \underline{\mathrm{n}}_{\mathrm{v}}[n] \tag{32}$$

where

$$\mathbb{H}_{\mathrm{v}} \triangleq \left[\underline{h}_{\mathrm{v},1}, \underline{h}_{\mathrm{v},2}, \ldots, \underline{h}_{\mathrm{v},K}\right]. \tag{33}$$

Based on the above, the virtual data matrix $\underline{\mathbb{X}}_{\mathrm{v}}$ can be expressed as follows:

$$\begin{aligned}\mathbb{X}_{\mathrm{v}} &= \left[\underline{x}_{\mathrm{v}}[1], \underline{x}_{\mathrm{v}}[2], \ldots, \underline{x}_{\mathrm{v}}[n], \ldots \underline{x}_{\mathrm{v}}\left[\mathcal{N}_{\mathrm{symb}}\right]\right] \\ &= \mathbb{M} \boxtimes \mathbb{X}_{\mathrm{ST}} \\ &= \underbrace{\left(\bar{\mathbb{S}}^{*} \boxtimes \mathbb{H}\right)}_{\mathbb{H}_{\mathrm{V}}}\mathrm{diag}\left\{\underline{\beta}\right\}\mathbb{F} + \underbrace{\mathbb{N}_{\mathrm{v}}}_{=\mathbb{M}\boxtimes\mathbb{N}_{\mathrm{ST}}}.\end{aligned} \tag{34}$$

As a result the second-order statistic of the proposed spatiotemporal-virtual received signal can expressed as follows:

$$\mathbb{R}_{x_{\mathrm{v}}x_{\mathrm{v}}} = \frac{1}{\mathcal{N}_{\mathrm{symb}}}\mathbb{X}_{\mathrm{v}}\mathbb{X}_{\mathrm{v}}^{H} \tag{35}$$

where the theoretical covariance matrix of the virtual noise is

$$\mathbb{R}_{\mathrm{vv}} = \mathcal{E}\left\{\underline{\mathrm{n}}_{\mathrm{v}}[n]\,\underline{\mathrm{n}}_{\mathrm{v}}^{H}[n]\right\} = \sigma_{\mathrm{n}}^{2}\mathbb{I}_{2\mathcal{N}_c N\bar{N}}.$$

In summary, in the 2nd manifold extender, the observation space has been increased by an additional $\bar{N}$ times and thus the dimensionality of the observation space in the virtual case is $2\mathcal{N}_c N\bar{N}$.

IV. TARGET PARAMETRIC ESTIMATION

The overall estimation procedures proposed in this article are blind and based on the assumptions of plane wave propagation, known array geometries, and fully calibrated arrays. Furthermore, without loss of generality, all targets and the radar system are assumed to be located on the (x, y)-plane, which implies that the elevation angle ϕ is equal to zero. Based on the 3-D (three-dimensional) data cube shown in Fig. 12 (see Appendix-A) and the spatiotemporal snapshot $\underline{x}[n]$ modeled by the manifold extenders in (18), the following target parameters will be estimated: DOAs, delays, Doppler frequencies, and complex path coefficients. In general, the intersection of the array manifold (a nonlinear subspace describing the radar system and embedded in the observation space) with the signal subspace (a linear subspace describing the receiver's data) will provide the estimation of the parameters of interest. Based on the orthogonality between the signal subspace and noise subspace, these intersections can be found by searching the array manifold and finding the minimum values of the projections onto the noise subspace. Therefore, by using the following cost function, which uses the inverse of the norm squared of the projection, the parameters of interest can be found by searching for the maximum points

$$\xi\left(\theta, \mathcal{F}_{\mathrm{chip}}, l\right) \triangleq \frac{\underline{h}^{H}\left(\theta, \mathcal{F}_{\mathrm{chip}}, l\right)\underline{h}\left(\theta, \mathcal{F}_{\mathrm{chip}}, l\right)}{\underline{h}^{H}\left(\theta, \mathcal{F}_{\mathrm{chip}}, l\right)\mathbb{P}_{\mathrm{n}}\underline{h}\left(\theta, \mathcal{F}_{\mathrm{chip}}, l\right)} \tag{36}$$

where $\mathbb{P}_{\mathrm{n}}$ is defined as the projector onto the noise subspace.

However, the above exhaustive searching is computationally expensive. Therefore, in this article, a two-stage estimation is proposed, starting with a joint DOA-delay estimation, followed by 1-D search for the Doppler frequencies.

A. Joint DOA-Delay Estimation

In the first stage, the cost function for both "manifold extenders" is defined as follows for jointly estimating the DOAs and Delays for all the targets:

$$\xi_1(\theta, l) \triangleq \begin{cases} \dfrac{\left\|\underline{S}(\theta) \otimes \mathbb{J}^{l}\underline{\mathfrak{c}}\right\|^{2}}{\left(\underline{S}(\theta) \otimes \mathbb{J}^{l}\underline{\mathfrak{c}}\right)^{H}\mathbb{P}_{\mathrm{n}}\left(\underline{S}(\theta) \otimes \mathbb{J}^{l}\underline{\mathfrak{c}}\right)} \\ \dfrac{\left\|\bar{\underline{S}}^{*}(\theta) \otimes \underline{S}(\theta) \otimes \mathbb{J}^{l}\underline{\mathfrak{c}}\right\|^{2}}{\left(\bar{\underline{S}}^{*}(\theta) \otimes \underline{S}(\theta) \otimes \mathbb{J}^{l}\underline{\mathfrak{c}}\right)^{H}\mathbb{P}_{\mathrm{n_v}}\left(\bar{\underline{S}}^{*}(\theta) \otimes \underline{S}(\theta) \otimes \mathbb{J}^{l}\underline{\mathfrak{c}}\right)} \end{cases} \tag{37}$$

Note that in this case, the Doppler frequency over chips has been temporally removed from the manifold vectors $\underline{h}$ and $\underline{h}_{\mathrm{v}}$ [see (20) and (31)] respectively. It is important to point out that in (37) both cost functions (top for the 1st and bottom for the 2nd manifold extender) operate in a similar manner, but with different projectors $\mathbb{P}_{\mathrm{n}}$ and $\mathbb{P}_{\mathrm{n_v}}$ in the denominator calculated using the following equation:

$$\mathbb{P} = \mathbb{E}\left(\mathbb{E}^{H}\mathbb{E}\right)^{-1}\mathbb{E}^{H} = \mathbb{E}\mathbb{E}^{H}. \tag{38}$$

In (38), $\mathbb{E}$ contains all the eigenvectors that can be obtained by the eigendecomposition of the covariance matrix of the received signals of the above two manifold extenders, i.e., $\mathbb{R}_{xx,\mathrm{ST}}$ and $\mathbb{R}_{x_{\mathrm{v}}x_{\mathrm{v}}}$ given by (27) and (35).

Without loss of generality, targets are assumed not sharing the DOA and delay (range) at the same time. Furthermore, it is assumed that the number of targets K is known (e.g. it has been given by AIC or MDL criteria). Therefore, by using the cost function ξ_1, K peaks will be obtained for both cases, and the DOAs and delays of the K targets will be estimated.

B. Doppler Frequency Estimation

Next, by inserting the K estimated DOAs and delays $(\hat{\theta}, \hat{l})$ back into the corresponding extended manifolds for both cases $\underline{h}(\hat{\theta}, \hat{l}, \mathcal{F}_{\mathrm{chip}})$ and $\underline{h}_{\mathrm{v}}(\hat{\theta}, \hat{l}, \mathcal{F}_{\mathrm{chip}})$, only the Doppler frequency remains unknown, which can be simply estimated by using the following 1-D search with respect to the

Doppler frequency over chips:

$$\xi_2\left(\mathcal{F}_{\text{chip}}\right) \triangleq \begin{cases} \sum_{k=1}^{K} \dfrac{\underline{h}_k^H\left(\mathcal{F}_{\text{chip}}\right)\underline{h}_k\left(\mathcal{F}_{\text{chip}}\right)}{\underline{h}_k^H\left(\mathcal{F}_{\text{chip}}\right)\mathbb{P}_{\text{n}}\underline{h}_k\left(\mathcal{F}_{\text{chip}}\right)} \\ \sum_{k=1}^{K} \dfrac{\underline{h}_{\text{v},k}^H\left(\mathcal{F}_{\text{chip}}\right)\underline{h}_{\text{v},k}\left(\mathcal{F}_{\text{chip}}\right)}{\underline{h}_{\text{v},k}^H\left(\mathcal{F}_{\text{chip}}\right)\mathbb{P}_{\text{n}_{\text{v}}}\underline{h}_{\text{v},k}\left(\mathcal{F}_{\text{chip}}\right)} \end{cases}. \quad (39)$$

It is also worth noting that other combinations of cost functions are also applicable, using however, different ways of data reshaping approaches. For instance in [23], the estimation is conducted by first joint Doppler-delay, followed by DOA based on a different data-reshaping procedure.

C. Complex Fading Coefficient Estimation

First manifold extender: Based on (24) and taking $\mathcal{N}_{\text{symb}}$ samples, the complex path fading coefficients $\underline{\beta}$ can be calculated by the following expression:

$$\underline{\hat{\beta}} = \underline{\text{diag}}\left\{\hat{\mathbb{H}}^{\#}\mathbb{X}_{\text{ST}}\left[\hat{\mathbb{F}} \odot \left(\hat{\bar{\mathbb{S}}}^H\mathbb{M}\right)\right]^{\#}\right\} \quad (40)$$

where $\hat{(\cdot)}$ denotes the matrix or vector constructed by inserting the K sets of estimated parameters $(\underline{\hat{l}}, \underline{\hat{\theta}}, \underline{\hat{\mathcal{F}}}_{\text{chip}})$ from the previous steps, and $(\cdot)^{\#}$ represents the pseudoinverse operator.

Second manifold extender: In this case, based on (32), and evaluating the matrices $\hat{\mathbb{H}}[n]$ and $\mathbb{F}_{\text{symb}}[n]$ using the estimates from previous stages, the complex path fading coefficients $\underline{\beta}$ for K targets can be obtained from the following equation:

$$\underline{\hat{\beta}} = \frac{1}{\mathcal{N}_{\text{symb}}}\sum_{n=1}^{\mathcal{N}_{\text{symb}}}\left(\mathbb{A}[n]\,\hat{\mathbb{H}}_{\text{v}}[n]\,\text{diag}\left\{\underline{\hat{\mathcal{F}}}_{\text{symb}}[n]\right\}\right)^{\#}\underline{x}_{\text{v}}[n]. \quad (41)$$

V. COMPUTER SIMULATION STUDIES

The performances of the two manifold extenders and proposed estimation algorithms are examined in this section using computer simulation studies. It is assumed that both the Tx and Rx antenna arrays are considered to be located on the (x, y) plane having uniform circular array (UCA) geometries of eight and nine elements, respectively. The Cartesian coordinates of these two array geometries as well as the geometry of the virtual array are also shown in the Fig. 3.

Furthermore, the transmitted symbol sequences are generated by using Hadamard codes of length $\mathcal{N}_{\text{symb}} = 256$ while an m-sequence of length of 31 is employed. The radar is assumed to operate with carrier frequency equals 10 GHz and chip period of 8.138 μs. The reference signal-to-noise ratio is denoted as SNR_0 as

$$\text{SNR}_0 \triangleq \frac{\text{Tr}\left\{\mathbb{M}\mathbb{M}^H\right\}}{\sigma_{\text{n}}^2} = \frac{\bar{N}}{\sigma_{\text{n}}^2} \quad (42)$$

and the SNR of the kth target is calculated via following equation:

$$\text{SNR}_k \triangleq |\beta_k|^2\,\text{SNR}_0. \quad (43)$$

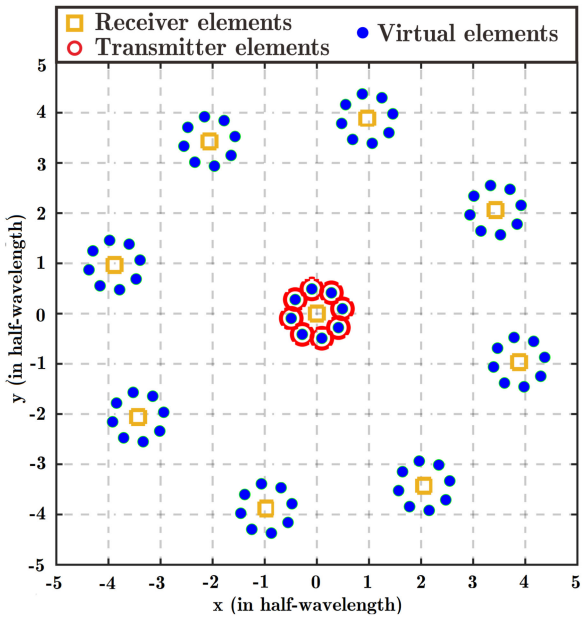

Fig. 3. Geometry of collocated MIMO radar. The UCA topology is implied on both transmitter array and receiver array with $N = 8$ and $\bar{N} = 9$. The unit of x and y axis is half wavelength.

TABLE II
MIMO Radar System Specification

Parameter	Symbol	Value
Elements of Tx Array	$\bar{N}$	8
Elements of Rx Array	N	9
Carrier Frequency	F_c	10 GHz (X-band)
Chip Period	T_c	8.138 μs
Reference SNR	SNR_0	20 dB
Primitive Polynomial	–	$D^5 + D^2 + 1$
Periods of m-sequence	$\mathcal{N}_c$	$2^5 - 1 = 31$
Tx Symbols	Symbols sequence	Hadamard code
Number of Tx Symbols	$\mathcal{N}_{\text{symb}}$	256

Other simulation parameters of this MIMO radar platform are given in Table II.

The radar operates in the presence of $K = 17$ moving targets. Without loss of generality, the targets are assumed on the same plane as the radar platform, i.e. only azimuth is considered, and distributed in the *far field* between 50° and 250°. The targets are assumed to move with velocities in the range of -40 and 40 m/s and their delays are between 1 T_c to 31 T_c. For each target, the magnitudes of the fading coefficients are selected from an Rayleigh distribution on the interval of $[\sqrt{0.1}, 1.2]$, the phase from a uniform distribution and the SNR_k of the kth target is assigned with the range of 0-10 dB. The received signal is corrupted by a white additive white Gaussian noise with zero mean and variance σ_{n}^2. The main target parameters are given in the Table III.

Numerical modeling of clutter is used in this article. The generation of the discrete signal snapshot $\underline{x}_{\text{c}}[n]$ can be done by following different distribution (according to the appli-

TABLE III
Targets' Environment

Target Index	Delay (T_c)	DOA (°)	Radial Velocity (m/s)	Fading Coefficient
1	10	239	14	0.47∠130°
2	8	166	-6	0.64∠138°
3	21	207	16	0.60∠140°
4	3	193	-20	0.41∠-55°
5	9	78	-34	0.28∠148°
6	9	189	3	0.45∠176°
7	28	129	-18	0.46∠51°
8	14	75	36	0.35∠-170°
9	24	178	33	0.34∠-43°
10	19	149	-9	0.80∠-132°
11	25	62	-38	0.74∠-154°
12	4	155	23	0.67∠-170°
13	31	113	27	1.02∠-42°
14	27	221	38	0.93∠-32°
15	2	51	-36	0.89∠161°
16	15	90	-4	1.09∠-145°
17	11	227	7	0.87∠-129°

cation), where in this article the *Weibull Distribution*[4] is used, generated via Matlab Statistical and Machine Learning Toolbox, with its scale parameter $\lambda = 1$ and shape parameter $k = 1.5$. The off-diagonals of the covariance $\mathbb{R}_{c,n}$ are not approximately zero, i.e., the clutter-plus-noise is no longer Gaussian, as this is shown in (44) at the bottom of this page.

Initially, the clutter preprocessing in Section II-D is conducted with the transformation matrix $\mathbb{T}$ is formed and applied on the received signal. Then the joint azimuth angles and delays estimation is examined using the cost function ξ_1. The searching steps are set as 1° for angles and $1T_c$ for delay. The results of both "Manifold Extender" approaches are shown in Figs. 4 and 5, where in the 3-D surf plots, 17 peaks can be clearly observed for both approaches. Two-dimensional views (azimuth-only and delay-only) are given in Fig. 6 for illustrative purposes. Comparing these estimated values with the true values in Table III indicates a successful azimuth–delay estimation.

Next, with the azimuth and delays correctly estimated, the velocities of the targets for both "Manifold Extender" approaches are estimated with the cost function ξ_2 using 1-D search with searching step of 0.5 m/s. The results are illustrated in the Fig. 7, where 17 peaks referring the target velocities can be clearly seen for the corresponding delays and azimuth.

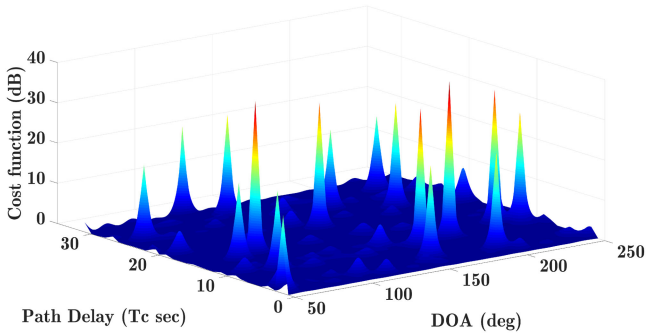

Fig. 4. Plot of the joint azimuth and delay estimation using the first "Manifold Extender" approaches.

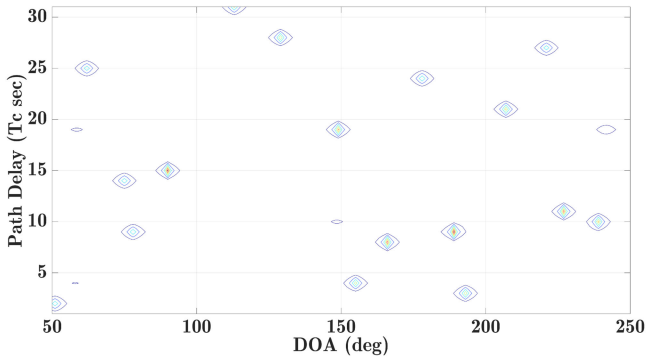

Fig. 5. Two-dimensional contour plot of the joint azimuth and delay estimation using the first "Manifold Extender" approach.

[4]The Weibull distribution is related to a number of other probability distributions, e.g. it interpolates between the exponential distribution ($k = 1$) and the Rayleigh distribution ($k = 2$ and $\lambda = \sqrt{2}\sigma$)

$$\mathbb{R}_{c,n} = \begin{bmatrix} 0.5024, & -0.0424, & -0.0001, & -0.0211, & -0.0176, & -0.0337, & -0.0412, & 0.0100, & 0.0059 \\ -0.0424, & 0.3317, & -0.0107, & -0.0003, & -0.0017, & 0.0150, & -0.0228, & 0.0180, & 0.0081 \\ -0.0001, & -0.0107, & 0.3377, & 0.0097, & 0.0030, & -0.0339, & -0.0195, & 0.0732, & 0.0002 \\ -0.0211, & -0.0003, & 0.0097, & 0.3848, & 0.0183, & -0.0256, & -0.0418, & -0.0243, & -0.0454 \\ -0.0176, & -0.0017, & 0.0030, & 0.0183, & 0.3258, & -0.0197, & 0.0041, & -0.0324, & 0.0136 \\ -0.0337, & 0.0150, & -0.0339, & -0.0256, & -0.0197, & 0.3157, & 0.0165, & -0.0313, & 0.0186 \\ -0.0412, & -0.0228, & -0.0195, & -0.0418, & 0.0041, & 0.0165, & 0.3279, & 0.0311, & 0.0167 \\ 0.0100, & 0.0180, & 0.0732, & -0.0243, & -0.0324, & -0.0313, & 0.0311, & 0.5069, & -0.0204 \\ 0.0059, & 0.0081, & 0.0002, & -0.0454, & 0.0136, & 0.0186, & 0.0167, & -0.0204, & 0.3547 \end{bmatrix}. \quad (44)$$

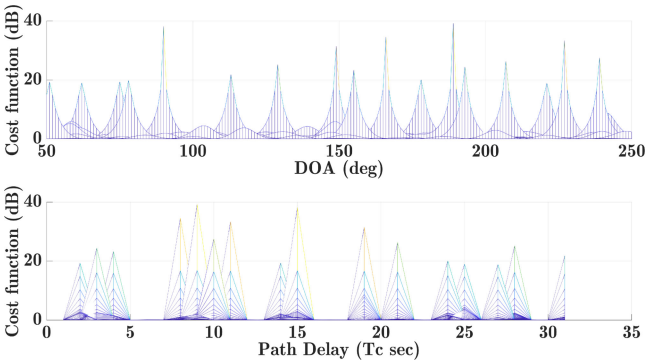

Fig. 6. Two-dimensional view of the azimuth estimation and delay estimation.

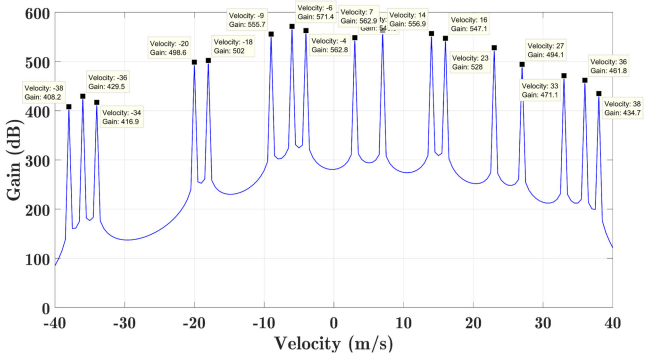

Fig. 7. One-dimensional subspace-based search for velocities using cost function ξ_2.

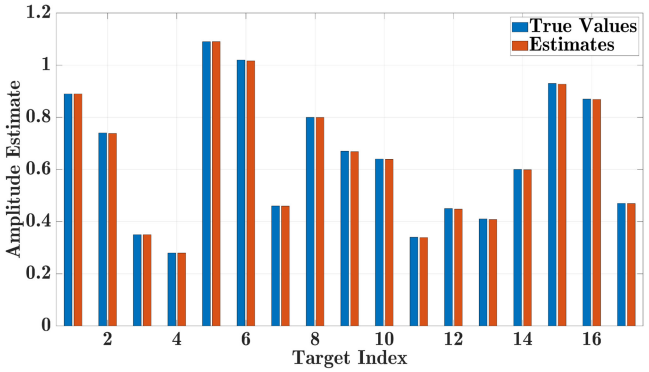

Fig. 8. Estimated complex coefficients magnitude for all 17 targets with the estimated value and true value indicated.

Indeed, using the estimates of DoA, delay, and velocity, the complex fading coefficients can be obtained by using (40) and (41), the results for magnitude and phase angle are presented in Figs. 8 and 9.

It is important to point out that conventional MIMO estimation algorithms such as LS, Capon, APES, CAPES, and CAML fail to provide results in the environment of the 17 targets described in Table III as the maximum number of targets for these algorithms is limited by the number $N = 9$. Note that the expression for above traditional parameter estimation algorithms are summarized in Table IV.

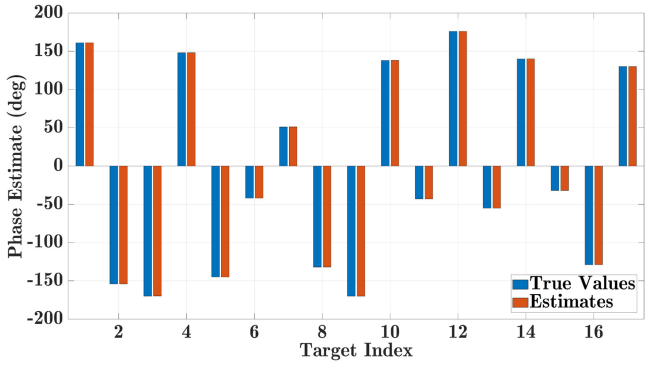

Fig. 9. Estimated complex coefficients phase for all 17 targets with the estimated value and true value indicated.

TABLE IV
Traditional MIMO Algorithms

LS	$\beta(\theta) = \dfrac{\underline{S}^H(\theta)\mathbb{R}_{xm}\overline{\underline{S}}(\theta)}{N\overline{N}}$
Capon	$\beta(\theta) = \dfrac{\underline{S}^H(\theta)\mathbb{R}_{xx}^{-1}\mathbb{R}_{xm}\overline{\underline{S}}(\theta)}{\overline{N}\underline{S}^H(\theta)\mathbb{R}_{xx}^{-1}\underline{S}(\theta)}$
APES	$\beta(\theta) = \dfrac{\underline{S}^H(\theta)\mathbb{Q}^{-1}\mathbb{R}_{xm}\overline{\underline{S}}(\theta)}{\overline{N}\underline{S}^H(\theta)\mathbb{Q}^{-1}\underline{S}(\theta)}$ where $\mathbb{Q} = \mathbb{R}_{xx} - \dfrac{1}{N}\mathbb{R}_{xm}\overline{\underline{S}}(\theta)\overline{\underline{S}}^H(\theta)\mathbb{R}_{xm}^H$
CAML	$\underline{\beta}(\underline{\theta}) = \left[\left(\mathbb{S}^H(\underline{\theta})\mathbb{T}^{-1}\mathbb{S}(\underline{\theta})\right) \odot \left(\overline{\mathbb{S}}^H(\underline{\theta})\mathbb{R}_{mm}\overline{\mathbb{S}}(\underline{\theta})\right)^T\right]^{-1}$.$\underline{\text{diag}}\left\{\mathbb{S}^H(\underline{\theta})\mathbb{T}^{-1}\mathbb{R}_{xm}\overline{\mathbb{S}}(\underline{\theta})\right\}$ where $\mathbb{T} = \mathbb{R}_{xx} - \mathbb{R}_{xm}\overline{\mathbb{S}}(\underline{\theta})\left(\overline{\mathbb{S}}^H(\underline{\theta})\mathbb{R}_{mm}\overline{\mathbb{S}}(\underline{\theta})\right)^{-1}$.$\overline{\mathbb{S}}^H(\underline{\theta})\mathbb{R}_{xm}^H$

Finally, the performance of the proposed approach is evaluated in terms of root-mean-square-error (RMSE) of the DOA θ and complex coefficients β using Monte–Carlo simulations with 2000 realizations. The expressions for estimating RMSEs are given as

$$\text{RMSE}_\theta = \frac{1}{K}\sum_{k=1}^{K}\sqrt{\mathcal{E}\left\{\left|\hat{\theta}_k - \theta_k\right|^2\right\}} \tag{45}$$

$$\text{RMSE}_\beta = \frac{1}{K}\sum_{k=1}^{K}\sqrt{\mathcal{E}\left\{\left|\hat{\beta}_k - \beta_k\right|^2\right\}}. \tag{46}$$

The number of Tx and Rx array elements are both reduced to five, for simplicity, with Cartesian coordinates

TABLE V
Target Parameters

Index	Delay (T_c)	DOA (°)	Coefficient
1	10	172.0201	$0.87\angle 10°$
2	8	156.5801	$0.94\angle -38°$
3	3	193.4201	$0.81\angle 55°$

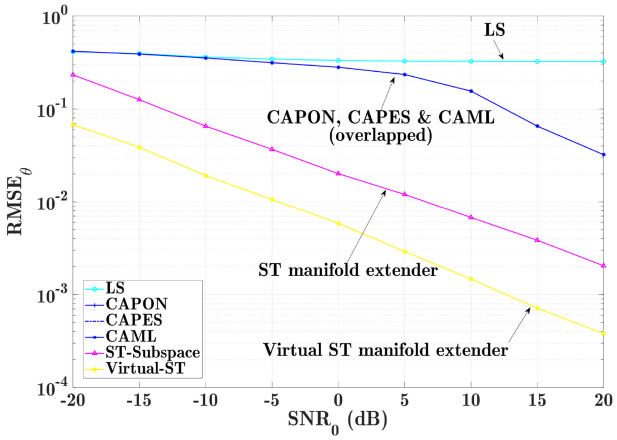

Fig. 10. RMSE$_\theta$ performance versus SNR$_0$ with the number of snapshots fixed at $2\mathcal{N}_{\text{symb}}\mathcal{N}_c$.

$$\text{Tx}: \begin{bmatrix} \underline{r}_x^T \\ \underline{r}_y^T \\ \underline{r}_z^T \end{bmatrix} = \begin{bmatrix} 0.2970, & -0.1907, & -0.4148, & -0.0657, & 0.3742 \\ 0.2970, & 0.3742, & -0.0657, & -0.4148, & -0.1907 \\ 0, & 0, & 0, & 0, & 0 \end{bmatrix}$$

$$\text{Rx}: \begin{bmatrix} \underline{r}_x^T \\ \underline{r}_y^T \\ \underline{r}_z^T \end{bmatrix} = \begin{bmatrix} -0.12, & -0.06, & 0, & 0.06, & 0.12 \\ 0, & 0, & 0, & 0, & 0 \\ 0, & 0, & 0, & 0, & 0 \end{bmatrix}$$

For a fair comparison, as the conventional MIMO algorithms are not able to handle "velocities" and number of targets more than N ($K > N$), three static targets are considered for all the methods with parameters given in Table V. The rest of the radar parameters are kept the same as shown in Table II.

The performance for both θ and β, i.e., RMSE$_\theta$ and RMSE$_\beta$ are illustrated respectively in Figs. 10 and 11. It is clear from both these figures that the two manifold extenders outperform the LS, CAPON, CAPES, and CAML algorithms.

VI. CONCLUSION

In this article, the novel concept of "Manifold Extender" is introduced, which increases the DoF of an arrayed MIMO radar. In particular, two "Manifold Extender" are presented in conjunction with a novel subspace-type framework for estimating the DOAs, delays, Doppler, and complex coefficients of a number of targets. The computer simulation

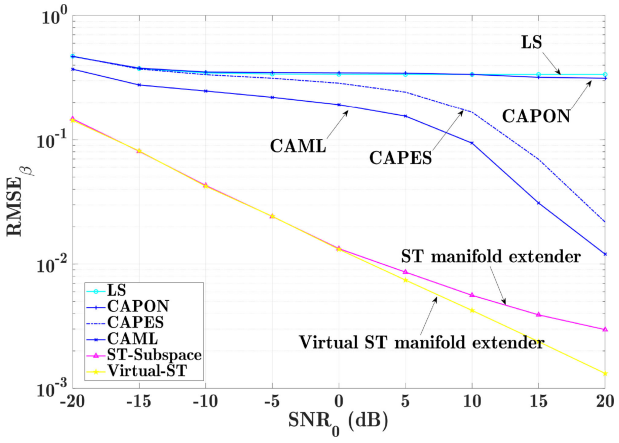

Fig. 11. RMSE$_\beta$ performance versus SNR$_0$ with the number of snapshots fixed at $2\mathcal{N}_{\text{symb}}\mathcal{N}_c$.

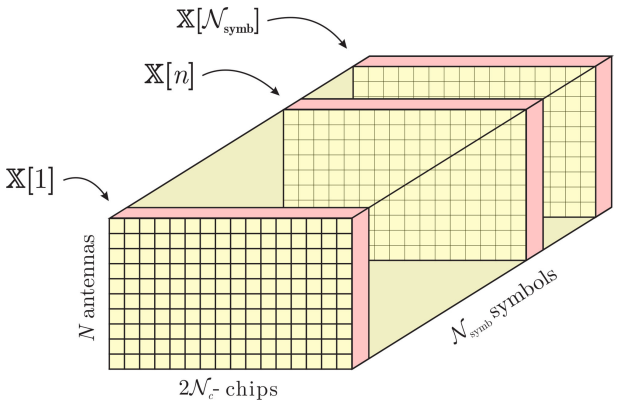

Fig. 12. Discretized received 3-D data cube.

studies show that both manifold extenders have better performance than other existing methods.

APPENDIX A
DERIVATION OF THE EQUATION (18)

According to (10), the discretized data $\mathbb{X}$

$$\mathbb{X} \triangleq \left[\mathbb{X}[1], \mathbb{X}[2], \ldots, \mathbb{X}[n], \ldots, \mathbb{X}\left[\mathcal{N}_{\text{symb}}\right]\right] \tag{47}$$

can be constructed as a 3-D data cube, with $\mathbb{X}[n] \in \mathcal{C}^{N\times 2\mathcal{N}_c}$ viewed as the nth slice of the 3-D cube as this is shown in Fig. 12. The martix $\mathbb{X}[n]$ is the discretized version of $\underline{x}(t)$ corresponding to the nth transmitted symbol interval

$$(n-1)\,T_{\text{symb}} \leqslant t \leqslant nT_{\text{symb}}.$$

and can be expressed as a function of the nth transmitted symbol $\underline{a}[n]$ as follows:

$$\mathbb{X}[n] = \sum_{k=1}^{K} \beta_k \underline{\mathcal{F}}_{\text{symb},k}[n]\, \underline{S}_k \bar{\underline{S}}_k^H \underline{a}[n] \left(\mathbb{J}^{l_k} \underline{c} \odot \underline{\mathcal{F}}_{\text{chip},k}\right)^T + \mathbb{N}[n]. \tag{48}$$

where the first term denotes the superposition of the signals from all the K targets. Then, the 3-D data cube is

transformed into a data matrix, denoted by $\mathbb{X}_{\mathrm{ST}}$:

$$\mathbb{X}_{\mathrm{ST}} \triangleq \left[\underline{x}\left[1\right], \underline{x}\left[2\right], \ldots, \underline{x}\left[n\right], \ldots, \underline{x}\left[\mathcal{N}_{\mathrm{symb}}\right]\right] \in \mathcal{C}^{2\mathcal{N}_c N \times \mathcal{N}_{\mathrm{symb}}} \tag{49}$$

whose nth column is defined as follows:

$$\underline{x}\left[n\right] \triangleq \mathrm{vec}\left(\mathbb{X}^T\left[n\right]\right) \in \mathcal{C}^{2\mathcal{N}_c N \times 1}. \tag{50}$$

Finally, using the following identities:

$$\mathrm{vec}\left(\mathbb{A}\mathbb{B}\mathbb{C}\right) = \left(\mathbb{C}^T \otimes \mathbb{A}\right)\mathrm{vec}\left(\mathbb{B}\right) \tag{51}$$

$$\left(\mathbb{A}\otimes\mathbb{B}\right)\left(\mathbb{C}\otimes\mathbb{D}\right) = \mathbb{A}\mathbb{C}\otimes\mathbb{B}\mathbb{D}. \tag{52}$$

and ignoring the noise term for mathematical simplicity, (50) can be rewritten as

$$\begin{aligned}
&\underline{x}\left[n\right] \triangleq \mathrm{vec}\left(\mathbb{X}^T\left[n\right]\right)\\
&= \mathrm{vec}\left(\left(\sum_{k=1}^{K}\beta_k \mathcal{F}_{\mathrm{s},k}\left[n\right]\underline{S}_k\bar{\underline{S}}_k^H\underline{\mathrm{a}}\left[n\right]\left(\mathbb{J}^{l_k}\underline{\mathrm{c}}\odot\underline{\mathcal{F}}_{\mathrm{c},k}\right)^T\right)^T\right)\\
&= \mathrm{vec}\left(\beta_k\mathcal{F}_{\mathrm{s},k}\left[n\right]\Big(\underbrace{\mathbb{J}^{l_k}\underline{\mathrm{c}}\odot\underline{\mathcal{F}}_{\mathrm{c},k}}_{\mathbb{A}}\Big)\underbrace{\underline{\mathrm{a}}^T\left[n\right]}_{\mathbb{B}}\Big(\underbrace{\underline{S}_k\bar{\underline{S}}_k^H}_{\mathbb{C}}\Big)^T\right)\\
&\overset{(51)}{=} \sum_{k=1}^{K}\beta_k\mathcal{F}_{\mathrm{s},k}\left[n\right]\left(\underline{S}_k\bar{\underline{S}}_k^H\otimes\left(\mathbb{J}^{l_k}\underline{\mathrm{c}}\odot\underline{\mathcal{F}}_{\mathrm{c},k}\right)\right)\underline{\mathrm{a}}\left[n\right]\\
&= \sum_{k=1}^{K}\beta_k\mathcal{F}_{\mathrm{s},k}\left[n\right]\left(\underline{S}_k\bar{\underline{S}}_k^H\otimes\left(\mathbb{J}^{l_k}\underline{\mathrm{c}}\odot\underline{\mathcal{F}}_{\mathrm{c},k}\right)1\right)\underline{\mathrm{a}}\left[n\right]\\
&\overset{(52)}{=} \sum_{k=1}^{K}\beta_k\,\mathcal{F}_{\mathrm{s},k}\left[n\right]\underbrace{\left(\underline{S}_k\otimes\left(\mathbb{J}^{l_k}\underline{\mathrm{c}}\odot\underline{\mathcal{F}}_{\mathrm{c},k}\right)\right)}_{\triangleq\underline{h}_k}\bar{\underline{S}}_k^H\,\underline{\mathrm{a}}\left[n\right]\\
&= \sum_{k=1}^{K}\beta_k\,\mathcal{F}_{\mathrm{s},k}\left[n\right]\underline{h}_k\bar{\underline{S}}_k^H\,\underline{\mathrm{a}}\left[n\right]
\end{aligned}$$

which results in (18). Note that in the previous equation $\mathcal{F}_{\mathrm{s},k}$ and $\underline{\mathcal{F}}_{\mathrm{c},k}$ denote the Doppler frequency over symbols and chips respectively (for notational simplicity).

APPENDIX B
DERIVATION OF EQUATIONS (29) AND (31)

Recall (18), by right-multiplying with the hermitian of the nth transmitted symbol vector $\underline{\mathrm{a}}[n]$ (outer product) and then "vectorization", we have:

$$\begin{aligned}
&\underline{x}_{\mathrm{v}}\left[n\right] \triangleq \mathrm{vec}\left(\underline{x}\left[n\right]\underline{\mathrm{a}}^H\left[n\right]\right)\\
&= \sum_{k=1}^{K}\beta_k\mathrm{vec}\Big\{\mathcal{F}_{\mathrm{s},k}\left[n\right]\left(\underline{S}_k\otimes\left(\mathbb{J}^{l_k}\underline{\mathrm{c}}\odot\underline{\mathcal{F}}_{\mathrm{c},k}\right)\right)\bar{\underline{S}}_k^H\,\underline{\mathrm{a}}\left[n\right]\underline{\mathrm{a}}^H\left[n\right]\Big\}\\
&= \sum_{k=1}^{K}\beta_k\mathrm{vec}\Big\{\mathcal{F}_{\mathrm{s},k}\left[n\right]\left(\underline{S}_k\otimes\left(\mathbb{J}^{l_k}\underline{\mathrm{c}}\odot\underline{\mathcal{F}}_{\mathrm{c},k}\right)\right)\left(\bar{\underline{S}}_k^H\otimes 1\right)\underline{\mathrm{a}}\left[n\right]\underline{\mathrm{a}}^H\left[n\right]\Big\}\\
&\overset{(52)}{=} \sum_{k=1}^{K}\beta_k\mathrm{vec}\Big\{\mathcal{F}_{\mathrm{s},k}\left[n\right]\left(\underline{S}_k\bar{\underline{S}}_k^H\otimes\left(\mathbb{J}^{l_k}\underline{\mathrm{c}}\odot\underline{\mathcal{F}}_{\mathrm{c},k}\right)\right)\left(\underline{\mathrm{a}}\left[n\right]\underline{\mathrm{a}}^H\left[n\right]\right)\Big\}\\
&= \sum_{k=1}^{K}\beta_k\mathrm{vec}\Big\{\mathcal{F}_{\mathrm{s},k}\left[n\right]\left(\underline{S}_k\bar{\underline{S}}_k^H\otimes\left(\mathbb{J}^{l_k}\underline{\mathrm{c}}\odot\underline{\mathcal{F}}_{\mathrm{c},k}\right)\right)\left(\underline{\mathrm{a}}\left[n\right]\underline{\mathrm{a}}^H\left[n\right]\right)\Big\}\\
&= \sum_{k=1}^{K}\beta_k\mathrm{vec}\Big\{\mathcal{F}_{\mathrm{s},k}\left[n\right]\mathbb{I}_{2\mathcal{N}_c N}\Big(\underline{S}_k\bar{\underline{S}}_k^H\otimes\Big(\mathbb{J}^{l_k}\underline{\mathrm{c}}\odot\underline{\mathcal{F}}_{\mathrm{c},k}\Big)\Big)\left(\underline{\mathrm{a}}\left[n\right]\underline{\mathrm{a}}^H\left[n\right]\right)\Big\}\\
&\overset{(51)}{=} \sum_{k=1}^{K}\beta_k\mathcal{F}_{\mathrm{s},k}\left[n\right]\underbrace{\left(\left(\underline{\mathrm{a}}\left[n\right]\underline{\mathrm{a}}^H\left[n\right]\right)^T\otimes\mathbb{I}_{2\mathcal{N}_c N}\right)}_{\triangleq\mathbb{A}[n]}\underbrace{\mathrm{vec}\left\{\underline{S}_k\bar{\underline{S}}_k^H\otimes\left(\mathbb{J}^{l_k}\underline{\mathrm{c}}\odot\underline{\mathcal{F}}_{\mathrm{c},k}\right)\right\}}_{\triangleq\underline{h}_{\mathrm{v},k}}\\
&= \sum_{k=1}^{K}\beta\mathbb{A}\left[n\right]\underline{h}_{\mathrm{v},k}\underline{\mathcal{F}}_{\mathrm{s},k}
\end{aligned}$$

which is equal to Eq. (29). Furthermore,

$$\begin{aligned}
\underline{h}_{\mathrm{v},k} &\triangleq \mathrm{vec}\left(\underline{S}_k\bar{\underline{S}}_k^H\otimes\left(\mathbb{J}^{l_k}\underline{\mathrm{c}}\odot\underline{\mathcal{F}}_{\mathrm{chip},k}\right)\right)\\
&\overset{(52)}{=} \mathrm{vec}\left(\left(\underline{S}_k\otimes\left(\mathbb{J}^{l_k}\underline{\mathrm{c}}\odot\underline{\mathcal{F}}_{\mathrm{chip},k}\right)\right)\bar{\underline{S}}_k^H\right)\\
&\overset{(51)}{=} \left(\bar{\underline{S}}_k^*\otimes\left(\underline{S}_k\otimes\left(\mathbb{J}^{l_k}\underline{\mathrm{c}}\odot\underline{\mathcal{F}}_{\mathrm{chip},k}\right)\right)\right)\mathrm{vec}(1)\\
&= \bar{\underline{S}}_k^*\otimes\underline{S}_k\otimes\left(\mathbb{J}^{l_k}\underline{\mathrm{c}}\odot\underline{\mathcal{F}}_{\mathrm{chip},k}\right)
\end{aligned}$$

which is equal to Eq. (31).

Note that for the spatiotemporal virtual noise, the covariance matrix can be formulated as

$$\begin{aligned}
\mathbb{R}_{\mathrm{n_v n_v}} &\triangleq \mathcal{E}\left\{\underline{\mathrm{n}}_{\mathrm{v}}\left[n\right]\underline{\mathrm{n}}_{\mathrm{v}}^H\left[n\right]\right\}\\
&= \mathcal{E}\left\{\left(\underline{\mathrm{a}}^*\left[n\right]\otimes\underline{\mathrm{n}}\left[n\right]\right)\left(\underline{\mathrm{a}}^*\left[n\right]\otimes\underline{\mathrm{n}}\left[n\right]\right)^H\right\}\\
&= \mathcal{E}\left\{\left(\underline{\mathrm{a}}^*\left[n\right]\otimes\underline{\mathrm{n}}\left[n\right]\right)\left(\underline{\mathrm{a}}^T\left[n\right]\otimes\underline{\mathrm{n}}^H\left[n\right]\right)\right\}\\
&\overset{(52)}{=} \mathcal{E}\left\{\left(\underline{\mathrm{a}}\left[n\right]\underline{\mathrm{a}}^H\left[n\right]\right)^T\otimes\left(\underline{\mathrm{n}}\left[n\right]\underline{\mathrm{n}}^H\left[n\right]\right)\right\}\\
&= \mathbb{I}_{\tilde{N}}\otimes\sigma_{\mathrm{n}}^2\mathbb{I}_{2\mathcal{N}_c N}\\
&= \sigma_{\mathrm{n}}^2\mathbb{I}_{2\mathcal{N}_c N\tilde{N}}.
\end{aligned}$$

REFERENCES

[1] E. M. Dowling and R. D. DeGroat
The equivalence of the total least squares and minimum norm methods
IEEE Trans. Signal Process., vol. 39, no. 8, pp. 1891–1892, Aug. 1991.

[2] J. Capon
High-resolution frequency-wavenumber spectrum analysis
Proc. IEEE, vol. 57, no. 8, pp. 1408–1418, Aug. 1969.

[3] J. Li and P. Stoica
MIMO radar with colocated antennas
IEEE Signal Process. Mag., vol. 24, no. 5, pp. 106–114, Sep. 2007.

[4] Z.-S. Liu, H. Li, and J. Li
Efficient implementation of capon and APES for spectral estimation
IEEE Trans. Aerosp. Electron. Syst., vol. 34, no. 4, pp. 1314–1319, Oct. 1998.

[5] J. L. P. Stoica and H. Li
A new derivation of the APES filter
IEEE Signal Process. Lett., vol. 6, no. 8, pp. 205–206, Aug. 1999.

[6] K. Luo and A. Manikas
Superresolution multitarget parameter estimation in MIMO radar
IEEE Trans. Geosci. Remote Sens., vol. 51, no. 6, pp. 3683–3693, Dec. 2012.

[7] L. Xu, J. Li, and P. Stoica
Radar imaging via adaptive MIMO techniques
In *Proc. 14th Euro. Signal Process. Conf.*, 2006, pp. 1–5.

[8] L. Xu, J. Li, and P. Stoica
Target detection and parameter estimation for MIMO radar systems
IEEE Trans. Aerosp. Electron. Syst., vol. 44, no. 3, pp. 927–939, Jul. 2008.

[9] F. C. Robey, D. R. Fuhrmann, E. J. Kelly, and R. Nitzberg
A CFAR adaptive matched filter detector
IEEE Trans. Aerosp. Electron. Syst., vol. 28, no. 1, pp. 208–216, Jan. 1992.

[10] L. Xu, P. Stoica, and J. Li
Parameter estimation and number detection of MIMO radar targets
In *Proc. Conf. Rec. 41st Asilomar Conf. Signals, Syst. Comput.*, 2007, pp. 177–181.

[11] R. Schmidt
Multiple emitter location and signal parameter estimation
IEEE Trans. Antennas Propag., vol. 34, no. 3, pp. 276–280, Apr. 1986.

[12] A. Manikas
Differential Geometry in Array Processing. London, U.K.: Imperial College Press, 2004.

[13] G. Efstathopoulos and A. Manikas
Extended array manifolds: Functions of array manifolds
IEEE Trans. Signal Process., vol. 59, no. 7, pp. 3272–3287, Jul. 2011.

[14] A. K. M. T. Rahman, S. M. M. H. Mahmud, T. K. Biswas, and S. Naznin
Target detection performance of coherent MIMO radar using space time adaptive processing
In *Proc. Int. Conf. Inform., Electron. Vis.*, Dhaka, Bangladesh, 2014, pp. 1–5.

[15] R. Lamare
Space-time adaptive beamforming algorithms for airborne radar systems
In *Beamforming - Sensor Signal Processing for Defence Applications*. London, U.K.: Imperial College Press, 2015, pp. 1–27.

[16] G. Hua and S. S. Abeysekera
Colocated MIMO radar transmit beamforming using orthogonal waveforms
In *Proc. IEEE Int. Conf. Acoust., Speech Signal Process.*, Kyoto, Japan, 2012, pp. 2453–2456.

[17] J. Xu, X. Dai, X. Xia, L. Wang, J. Yu, and Y. Peng
Optimal transmitting diversity degree-of-freedom for statistical MIMO radar
In *Proc. IEEE Radar Conf.*, Arlington, TX, USA, 2010, pp. 437–440.

[18] C. Y. Chong, F. Pascal, J. P. Ovarlez, and M. Lesturgie
MIMO radar detection in non-Gaussian and heterogeneous clutter
IEEE J. Sel. Topics Signal Process., vol. 4, no. 1, pp. 115–126, Jan. 2010.

[19] S. Watts
Radar detection prediction in K-distributed sea clutter and thermal noise
IEEE Trans. Aerosp. Electron. Syst., vol. AES-23, no. 1, pp. 40–45, Jan. 1987.

[20] L. Lei, X. Rongqing, and L. Gaopeng
Ionospheric clutter mitigation with knowledge aided pre-whiten in high frequency surface wave radar
In *Proc. IEEE Radar Conf.*, Boston, MA, USA, 2007, pp. 558–561.

[21] A. Manikas and M. Sethi
A space-time channel estimator and single-user receiver for code-reuse DS-CDMA systems
IEEE Trans. Signal Process., vol. 51, no. 1, pp. 39–51, Jan. 2003.

[22] A. Manikas and L. K. Huang
STAR channel estimation in DS-CDMA communication systems
IEE Proc. - Commun., vol. 151, no. 4, pp. 387–393, Aug. 2004.

[23] V. Sridhar, T. Gabillard and A. Manikas
Spatiotemporal-MIMO channel estimator and beamformer for 5G
IEEE Trans. Wireless Commun., vol. 15, no. 12, pp. 8025–8038, Sep. 2016.

He Ren received the B.Eng. degree from the Department of Electronics and Electronics Engineering, University of Bristol, U.K. in 2011, the M.Sc. degree from University College London, U.K., and the Ph.D. degree in 2018 from the Department of Electrical and Electronic Engineering, Imperial College London, U.K., under the supervision of Prof. A. Manikas.

He joined the CITI Group, New York, NY, USA, served as Quantitative Analyst in Rates Algorithm Trading, and currently, moved to the Quantitative Investment Strategy (CIS) team as a Strategist. His research interests include array signal processing and arrayed MIMO radar.

Athanassios Manikas (SM'02) holds the Chair of the Communications and Array Signal Processing with the Department of Electrical and Electronic Engineering, Imperial College London, London, U.K. He has held a number of research consultancies for the EU, industry, and government organisations. He is leading a strong group of researchers at Imperial College and has successfully supervised more than 50 Ph.D.'s and 200 master's project-students. He has authored and coauthored an extensive set of journal and conference papers in the areas of wireless communications and array signal processing and is the author of a monograph entitled *Differential Geometry in Array Processing*. His main research interests include space-time wireless communications, antenna arrays, array signal processing, beamforming, localization, uncertainties, mathematical modeling, analysis and algorithmic design, radar signal processing, MIMO radar, wireless sensor networks, 5G+, and physical layer.

Dr. Manikas is a Fellow of the Institution of Engineering and Technology (IET), Fellow of the Institute of Mathematics and its Applications (IMA), and he was a Distinguished Lecturer of IEEE Communications Society (2016–2017). He was also the Chair of IEEE COMSOC TAOS Technical Committee (2017–2018). He is on various Editorial Boards and has had various technical chairs at international conferences, including the TPC Chair of IEEE International Conference on Communications, 2015 in London.